

Taylor dispersion in the presence of cross flow and interfacial mass transferTiras Y. Lin^{1,*} and Eric S. G. Shaqfeh^{1,2,3,†}¹*Department of Mechanical Engineering, Stanford University, Stanford, California 94305, USA*²*Department of Chemical Engineering, Stanford University, Stanford, California 94305, USA*³*Institute for Computational and Mathematical Engineering, Stanford University, Stanford, California 94305, USA*

(Received 29 October 2018; published 1 March 2019)

Transverse velocity gradients can enhance the effective diffusion coefficient of a scalar in the primary flow direction, a phenomenon known colloquially as Taylor dispersion. In this work, we perform Taylor dispersion analysis on a canonical pressure-driven flow in a channel with a cross flow, using both perturbation theory and Brownian dynamics simulations. Moreover, we illustrate how mass transfer at the wall affects the evolution of the scalar. By writing a one-dimensional advection-diffusion-mass-transfer equation for the cross-sectionally averaged concentration, we elucidate how the effective diffusion coefficients, effective advective velocities, and effective mass-transfer rates depend on the strength of the cross flow and the wall transfer coefficient. We perform an asymptotic analysis to investigate the limit of strong cross flow and demonstrate that, in this limit, dispersion rapidly decreases with increasing cross-flow velocity V as V^{-4} and scales with the Brownian diffusivity D as D^3 . Additionally, we discuss the effect of the Schmidt number, the ratio of momentum to mass diffusion, which effectively controls the extent to which the cross flow affects the axial velocity profile. Finally, we describe how our results can be extended to include transverse velocities and diffusivities that are spatially nonuniform.

DOI: [10.1103/PhysRevFluids.4.034501](https://doi.org/10.1103/PhysRevFluids.4.034501)**I. INTRODUCTION**

In 1953, Taylor [1] showed that a scalar flowing in a circular pipe experiences an enhanced effective axial diffusion coefficient. The phenomenon—also shown by studying moments of the scalar distribution by Aris [2]—is a result of the coupling between velocity gradients in the transverse direction with Brownian motion of the solute. Since this original work, many problems extending the classical Taylor dispersion analysis have been posed and solved, where the goal is typically to write an equation that governs the cross-sectionally averaged concentration of a solute. For example, Taylor [3] extended his analysis to the case of turbulent flow, Nadim *et al.* [4] studied the transport of a sedimenting solute in a pressure-driven pipe flow that is slowly rotated about its axis of symmetry, Erdogan and Chatwin [5] analyzed the effect of a Dean flow on Taylor dispersion in a gently curving pipe, and James and Chrysikopoulos [6] illustrated how the finite size of a particle affects the dispersion properties.

Taylor dispersion analysis has also been extended to include the case where the solute adsorbs to the walls [7–12]. Notably, Shapiro and Brenner [13] extended generalized Taylor dispersion analysis [14] to include curvilinear flow, applied external forces on the solute, and spatially nonuniform reaction constants. This work was further extended by Shapiro and Brenner [15], and in the latter work, they considered the specific example of Brownian particles sedimenting under gravity in a

*tiraslin@stanford.edu

†esgs@stanford.edu

Poiseuille flow between two parallel plates, where the bottom plate is reactive. When reaction is negligible, they show that the Taylor dispersion coefficient increases slightly as the sedimentation velocity increases slightly.

In general, any driving force causing the solute to move in the direction orthogonal to the primary flow direction within a channel would be expected to affect Taylor dispersion analysis in a nontrivial fashion. Such a situation arises, for example, in cross-flow filtration, where a starting solution flows through a porous channel and a pressure difference across the porous wall—the filter—drives the permeate out [16]. Essentially, this system is a leaky pipe where the cross flow is set by an applied pressure difference. A related flow occurs in the treatment of a cancerous tumor using nanoparticles. It is well known that the walls of tumor blood vessels are porous [17] and that drug-delivery nanoparticles can extravasate through these pores. Interactions with red blood cells drive nanoparticles toward the blood vessel walls, where there is a red blood cell-free layer [18]. As in the cross-flow filtration example, pressure gradients across the blood vessel wall can drive a suction flow, either inwards or outwards, carrying particles with it [19]. Additionally, the use of a strong applied magnetic field has been shown to be a promising method to direct magnetic nanoparticles to specific tumor sites [20,21], which drives particle motion orthogonal to the primary direction of blood flow. The mass transfer across the porous blood vessel wall dictates the efficacy of the drug-delivery nanoparticles [22], thus highlighting the importance of understanding how cross flow and interfacial mass transfer affect particle transport.

In the present work, we study the transport of Brownian point particles in a channel with porous walls, advected by a pressure-driven flow and a uniform cross flow in the transverse direction. The cross flow advects the particles toward the bottom wall, which may or may not be then transferred across the wall. Using both perturbation theory and Brownian dynamics simulations, we determine the effective Taylor dispersion coefficient, effective velocity, and effective mass-transfer rate of the cross-sectionally averaged particle concentration. Additionally, we elucidate the asymptotic behavior of particle transport in the regime of strong cross flow, and we illustrate how the ratio of momentum diffusivity to particle diffusivity, i.e., the Schmidt number, affects particle transport. By considering the limit of infinite Schmidt number and weak cross flow, we show that our work corresponds to the example of sedimenting Brownian particles given by Shapiro and Brenner [15], but our results differ significantly. Importantly, as noted previously, they report an increase in dispersivity with a mild increase in sedimentation velocity, but in fact we show that subsequent increases in the cross-flow velocity actually lead to a rapid decrease in dispersivity. Finally, we describe how our results can be extended to take into account a nonuniform transverse velocity and diffusivity, since most cross flows in realistic settings are not spatially uniform. We describe applications where this situation might arise and demonstrate the utility of our results by showing how the lateral migration of particles in a viscoelastic channel flow affects dispersion properties.

II. PROBLEM SETUP AND METHODOLOGY

In order to investigate the effect of cross flow and wall mass transfer on the Taylor dispersion of a scalar, we consider a canonical pressure-driven incompressible flow in a 2D channel of height H with porous walls. A pressure gradient $-dp/dx$ drives flow through the channel in the x direction, and a constant, uniform cross-flow velocity V is supplied in the $-y$ direction. The velocity field in the channel, described pedagogically by Batchelor [23], pp. 282–285, is given by $\mathbf{u} = u(y)\hat{\mathbf{i}} + v\hat{\mathbf{j}}$ and is shown in Fig. 1(a). In particular,

$$u(y) = -\frac{dp}{dx} \frac{1}{\rho V} \left[-y + H \frac{1 - \exp(-Vy/\nu)}{1 - \exp(-VH/\nu)} \right], \quad (1a)$$

$$v = -V, \quad (1b)$$

where ρ and ν are the fluid density and kinematic viscosity, respectively. We note that when $V = 0$, the flow reduces to plane Poiseuille flow.

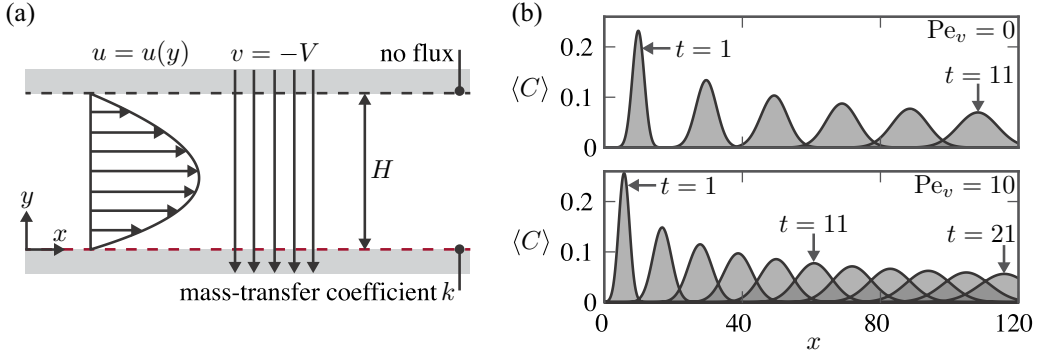


FIG. 1. (a) Schematic of the problem considered. A pressure gradient drives flow through the channel in the x direction ($\text{Re}_v = 1$ shown), and a constant, uniform cross-flow velocity V is supplied in the $-y$ direction. No flux is permitted at the top wall, and the scalar is transferred with a dimensional mass-transfer coefficient k , or dimensionless Sherwood number Sh , at the bottom wall. (b) Cross-sectionally averaged concentration $\langle C \rangle$ is shown when $\text{Pe}_u = 10$ for $\text{Pe}_v = 0$ (top) and $\text{Pe}_v = 10$ (bottom) at several times, in increments of $\Delta t = 2$, with a delta function initial condition. Numerically determined histograms are shown in gray, and best-fit Gaussians are shown in black.

The scalar has a concentration field $C = C(x, y, t)$, and it is advected by the velocity field given above and diffuses with a Brownian diffusion coefficient D . At the bottom wall ($y = 0$), the scalar is transferred across the wall with first-order mass-transfer coefficient k , and at the top wall ($y = H$), no flux is permitted.

We make our equations dimensionless with

$$u = Uu^*, \quad v = Vv^*, \quad x = Hx^*, \quad y = Hy^*, \quad t = \frac{H^2}{D}t^*, \quad C = C_iC^*, \quad (2)$$

where $U = -(dp/dx)H^2/12\rho\nu$ is the average velocity in the x direction across the channel when $V = 0$, C_i is a characteristic initial concentration, and the asterisk denotes a dimensionless quantity. This procedure yields four dimensionless numbers,

$$\text{Pe}_u = \frac{UH}{D}, \quad \text{Pe}_v = \frac{VH}{D}, \quad \text{Re}_v = \frac{VH}{\nu}, \quad \text{Sh} = \frac{kH}{D}, \quad (3)$$

where the first two are Péclet numbers based on U and V , respectively, the third is a Reynolds number based on V , and the fourth is a Sherwood number. The Schmidt number is $\text{Sc} = \nu/D$, so by definition, $\text{Pe}_v = \text{Re}_v\text{Sc}$. Henceforth, we omit the asterisk used to denote a nondimensional quantity to simplify the notation, unless otherwise noted.

The scalar concentration field is governed by the following dimensionless Fokker-Planck equation:

$$\frac{\partial C}{\partial t} + \text{Pe}_u u(y) \frac{\partial C}{\partial x} - \text{Pe}_v \frac{\partial C}{\partial y} = \frac{\partial^2 C}{\partial x^2} + \frac{\partial^2 C}{\partial y^2}, \quad (4a)$$

$$\frac{\partial C}{\partial y} + \text{Pe}_v C = \{\text{Sh} C, 0\}, \quad \text{at } y = \{0, 1\}, \quad (4b)$$

where the dimensionless velocity in the x direction is

$$u(y) = \frac{12}{\text{Re}_v} \left[-y + \frac{1 - \exp(-\text{Re}_v y)}{1 - \exp(-\text{Re}_v)} \right]. \quad (5)$$

When $\text{Sh} = 0$, there is no mass transfer through the bottom wall, and both walls are thus no flux boundaries. In the first part of this paper, we hold Re_v fixed at $\text{Re}_v = 1$. In doing so, the strength of

the cross flow is effectively decoupled from the axial flow: as Pe_v increases, Sc increases accordingly to enforce a fixed Re_v and the velocity field shown in Eq. (5) remains the same. In Sec. III F, we will discuss the effect of holding Sc fixed: an increase in Pe_v now requires a simultaneous increase in Re_v , and based on the velocity field, the magnitude of Re_v controls the extent to which the maximum of $u(y)$ moves toward the bottom wall. We perform Taylor dispersion analysis on Eqs. (4a) and (4b) using two different methods: Brownian dynamics (BD) simulations and perturbation theory. The BD simulations serve as a validation of our theory.

First, we describe our BD simulations. The stochastic differential equations corresponding to Eq. (4a) are

$$dx = Pe_u u(y) dt + \sqrt{2} dW, \quad (6a)$$

$$dy = -Pe_v dt + \sqrt{2} dW, \quad (6b)$$

where dW are Gaussian random numbers with mean 0 and variance dt . To analyze the evolution of the concentration field, many point particles are randomly distributed across the channel at $x = 0$ at time $t = 0$ (i.e., a delta function in time and space), and the trajectories of the point particles are evolved according to Eqs. (6a) and (6b) using the Euler-Maruyama scheme [24]; when $Sh = 0$, we simulate 2.5×10^3 particles and use a time step of $dt = 10^{-4}$, and when $Sh \neq 0$, we simulate 10^6 particles and use a time step of $dt = 10^{-5}$. When a particle is detected to have crossed the top wall at $y = 1$, it is reflected back into the domain, and when a particle is detected to have crossed the bottom wall at $y = 0$, it is reflected back into the domain with probability $1 - Sh\sqrt{\pi dt}$ or considered transferred out of the channel otherwise [25]. This procedure corresponds to the boundary conditions given in Eq. (4b) (also see Ref. [22] for an example of this boundary condition used to study extravasation of nanoparticles).

To visualize the results of the BD simulations, we analyze the cross-sectionally averaged concentration field. Let cross-sectionally averaged quantities be denoted by

$$\langle \cdot \rangle = \int_0^1 \cdot dy. \quad (7)$$

In Fig. 1(b), the cross-sectionally averaged concentration $\langle C \rangle(x, t)$ is plotted for $Pe_u = 10$ and $Sh = 0$ for two cases: $Pe_v = 0$ (top) and $Pe_v = 10$ (bottom). The numerically determined histograms of particle concentrations are shown in gray and a best-fit Gaussian is shown as a thin black line; $\langle C \rangle$ is shown at several times, in increments of $\Delta t = 2$. Not surprisingly, $\langle C \rangle$ evolves as a Gaussian when $Pe_v = 0$, the solution to a 1D advection-diffusion equation with a delta function initial condition. We observe that the same occurs when there is cross flow—albeit translating more slowly with a seemingly smaller effective diffusion coefficient—suggesting that the effective Taylor dispersion coefficient D_{TD} , effective velocity $\langle u \rangle_{\text{eff}}$, and effective Sherwood number Sh_{eff} (when $Sh \neq 0$) depend on the dimensionless numbers in a nontrivial way.

Ultimately, we are interested in describing the evolution of $\langle C \rangle$ with a one-dimensional advection-diffusion-mass-transfer equation,

$$\frac{\partial \langle C \rangle}{\partial t} + Pe_u \langle u \rangle_{\text{eff}} \frac{\partial \langle C \rangle}{\partial x} = \left(1 + \frac{D_{TD}}{D} \right) \frac{\partial^2 \langle C \rangle}{\partial x^2} - Sh_{\text{eff}} \langle C \rangle, \quad (8)$$

which has the well-known Green's function

$$\langle C \rangle = \frac{1}{\sqrt{4D_{\text{eff}}t}} \exp \left[-\frac{(x - \langle u \rangle_{\text{eff}} Pe_u t)^2}{4D_{\text{eff}}t} - Sh_{\text{eff}} t \right], \quad (9)$$

where $D_{\text{eff}} = 1 + D_{TD}/D$, representing a point release of scalar at $x = 0$ and $t = 0$. In order to make theoretical progress, we recognize that the extent of spreading in the x direction goes like $\sim \sqrt{D_{TD}t}$, which at long times is much larger than H . Instead of the nondimensionalizations for x^* and t^* presented in Eq. (2), we scale x as $x = L\bar{x}$ and t as $t = (L^2/D_{TD})\bar{t}$ instead, where L is a

characteristic width of spreading that is $\gg H$. With these new scalings, Eq. (4a) is

$$\delta^2 \frac{D_{TD}}{D} \frac{\partial C}{\partial \bar{t}} + \delta \text{Pe}_u u(y) \frac{\partial C}{\partial \bar{x}} - \text{Pe}_v \frac{\partial C}{\partial y} = \delta^2 \frac{\partial^2 C}{\partial \bar{x}^2} + \frac{\partial^2 C}{\partial y^2}, \quad (10)$$

where $\delta = H/L$ is the aspect ratio of the channel height to the extent of spreading, and the boundary conditions in Eq. (4b) remain unchanged. By taking the cross-sectional average of Eq. (10) and enforcing the boundary conditions, we have

$$\delta^2 \frac{D_{TD}}{D} \frac{\partial \langle C \rangle}{\partial \bar{t}} + \delta \text{Pe}_u \frac{\partial \langle uC \rangle}{\partial \bar{x}} = \delta^2 \frac{\partial^2 \langle C \rangle}{\partial \bar{x}^2} - \text{Sh} C(y=0). \quad (11)$$

Akin to Taylor's analysis, we consider the solution at long times, when $\delta \ll 1$. We seek to model the $\partial \langle uC \rangle / \partial \bar{x}$ term, which will have two components: one which enhances the effective diffusion coefficient (Taylor dispersion), and one which alters the effective advective velocity. In order to do so, we expand C as a dual perturbation series:

$$C = C_0 + \delta C_1^\delta + \text{Sh} C_1^{\text{Sh}} + \dots \quad (12)$$

By substituting this expansion in Eqs. (10) and (4b), we can pose the problems at $O(1)$, $O(\delta)$, and $O(\text{Sh})$. At $O(1)$, we have

$$O(1) : \quad \frac{\partial^2 C_0}{\partial y^2} + \text{Pe}_v \frac{\partial C_0}{\partial y} = 0, \quad (13a)$$

$$\frac{\partial C_0}{\partial y} + \text{Pe}_v C_0 = 0, \quad \text{at } y = 0, 1. \quad (13b)$$

By enforcing that $\langle C \rangle = \langle C_0 \rangle$ (or equivalently, that the cross-sectional average of the higher order corrections is zero), we have

$$C_0 = \langle C \rangle \mathcal{P}(y), \quad (14)$$

where for a delta function initial condition, $\langle C \rangle = \langle C \rangle(x, t)$ is given by Eq. (9), and where

$$\mathcal{P}(y) = \frac{\text{Pe}_v \exp(-\text{Pe}_v y)}{1 - \exp(-\text{Pe}_v)} \quad (15)$$

serves as a weighting function for the concentration field. Immediately, we observe that at this order, $\langle C \rangle$ is not simply advected by $\langle u \rangle$ since the scalar is not distributed uniformly across the width of the channel. We define the deviation from this zeroth-order effective velocity as

$$\tilde{u}(y) = u(y) - \int_0^1 \mathcal{P}(y) u(y) dy. \quad (16)$$

With the $O(1)$ solution, we now proceed to pose the $O(\delta)$ and $O(\text{Sh})$ problems, which are

$$O(\delta) : \quad \frac{\partial^2 C_1^\delta}{\partial y^2} + \text{Pe}_v \frac{\partial C_1^\delta}{\partial y} = \text{Pe}_u \tilde{u}(y) \frac{\partial C_0}{\partial \bar{x}}, \quad (17a)$$

$$\frac{\partial C_1^\delta}{\partial y} + \text{Pe}_v C_1^\delta = 0, \quad \text{at } y = 0, 1, \quad (17b)$$

$$O(\text{Sh}) : \quad \frac{\partial^2 C_1^{\text{Sh}}}{\partial y^2} + \text{Pe}_v \frac{\partial C_1^{\text{Sh}}}{\partial y} = -\mathcal{P}(0) C_0, \quad (17c)$$

$$\frac{\partial C_1^{\text{Sh}}}{\partial y} + \text{Pe}_v C_1^{\text{Sh}} = \{C_0, 0\}, \quad \text{at } y = \{0, 1\}. \quad (17d)$$

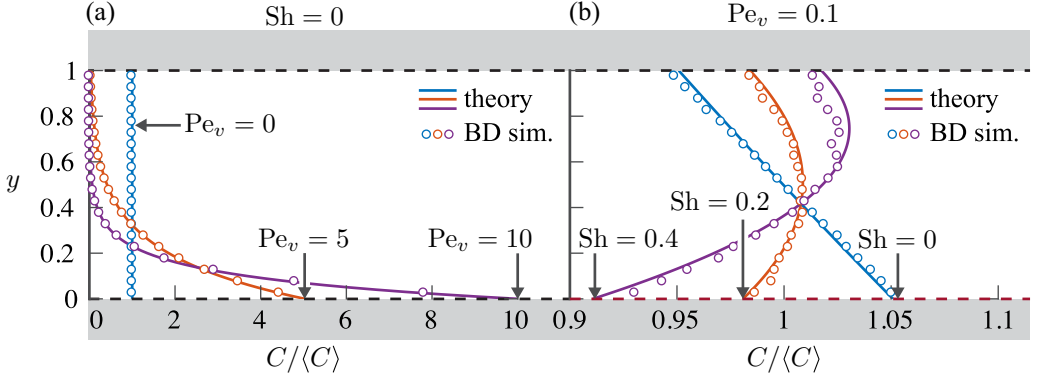


FIG. 2. Concentration profiles $C/\langle C \rangle$ when $Pe_u = 10$ and $Re_v = 1$ are shown for (a) $Sh = 0$, $Pe_v = \{0, 5, 10\}$, and (b) $Pe_v = 0.1$, $Sh = \{0, 0.2, 0.4\}$. In BD simulations, concentration profiles at the center of the traveling Gaussian are averaged over time.

Importantly, while $\partial\langle C \rangle/\partial x$ drives the solution for C_1^δ , $\langle C \rangle$ drives the solution for C_1^{Sh} . Based on this, we expect C_1^δ to control the Taylor dispersion coefficient and C_1^{Sh} to control the effective Sherwood number and further alter the effective velocity.

III. RESULTS AND DISCUSSION

A. The concentration field

Using integrating factors, the solution for the concentration is determined to be

$$C = \langle C \rangle \mathcal{P}(y) + Sh \langle C \rangle \mathcal{P}(y) \mathcal{Q}(y) + \frac{\partial\langle C \rangle}{\partial x} Pe_u \exp(-Pe_v y) \left\{ \int_0^y \exp(Pe_v \sigma) \left[\int_0^\sigma \mathcal{P}(\xi) \tilde{u}(\xi) d\xi \right] d\sigma + A(x, t) \right\}, \quad (18)$$

where $A(x, t)$ is a constant that enforces the condition that $\int_0^1 C_1^{Sh} dy = 0$, but is inconsequential for our results in this work as we will show in our discussion on the Taylor dispersion coefficient, and

$$\mathcal{Q}(y) = \frac{\exp(Pe_v) Pe_v y - \exp(Pe_v y) + 1}{[\exp(Pe_v) - 1] Pe_v} + \frac{\sinh(Pe_v) - Pe_v}{[1 - \cosh(Pe_v)] Pe_v} \quad (19)$$

is another weighting function associated with mass transfer. In Figs. 2(a) and 2(b) we show concentration profiles as a function of y from Eq. (18) and our BD simulations. Specifically, we show the concentration profile at the center of the Gaussian averaged over time, which is simply $C/\langle C \rangle = \mathcal{P}(y) + Sh \mathcal{P}(y) \mathcal{Q}(y)$, because $\partial\langle C \rangle/\partial x = 0$ there. In Fig. 2(a), $C/\langle C \rangle$ is shown for $Sh = 0$ and $Pe_v = \{0, 5, 10\}$; as the strength of the cross flow increases, the majority of the concentration is pushed closer to the bottom wall. In Fig. 2(b), $C/\langle C \rangle$ is shown for $Pe_v = 0.1$ and $Sh = \{0, 0.2, 0.4\}$; as Sh increases, more and more concentration close to the wall is transferred, leading to a depletion close to the wall.

B. The Taylor dispersion coefficient

Based on the solution for the concentration given in Eq. (18), we may now examine how the $\partial\langle uC \rangle/\partial \bar{x}$ term in Eq. (11) affects the effective diffusion coefficient. In particular, by substituting the portion of the concentration that depends on $\partial\langle C \rangle/\partial x$ into this term, we arrive at an extra diffusion term $(D_{TD}/D) \partial^2 \langle C \rangle / \partial x^2$, where the Taylor dispersion coefficient is

$$\frac{D_{TD}}{D} = -Pe_u^2 \int_0^1 \tilde{u}(y) \exp(-Pe_v y) \left\{ \int_0^y \exp(Pe_v \sigma) \left[\int_0^\sigma \mathcal{P}(\xi) \tilde{u}(\xi) d\xi \right] d\sigma \right\} dy. \quad (20)$$

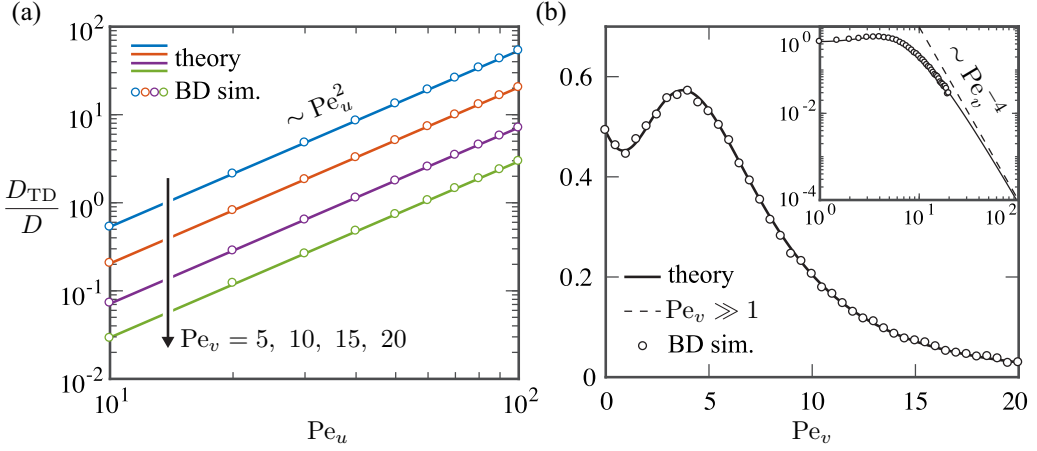


FIG. 3. Taylor dispersion coefficients D_{TD}/D in the absence of mass transfer, $\text{Sh} = 0$, and when $\text{Re}_v = 1$ are shown as functions of (a) Pe_u , for $\text{Pe}_v = \{5, 10, 15, 20\}$, and (b) Pe_v , for $\text{Pe}_u = 10$. The inset shows the asymptotic behavior of the dispersion coefficient when $\text{Pe}_v \gg 1$.

The constant $A(x, t)$ in the concentration field does not affect the dispersion coefficient, since $\int_0^1 \tilde{u}(y) \exp(-\text{Pe}_v y) dy = 0$. We note that in the absence of cross flow, we recover the classical result for plane Poiseuille flow, $D_{\text{TD}}/D = \text{Pe}_u^2/210$, and interestingly, D_{TD}/D is not affected by the $O(\text{Sh})$ perturbation. In Figs. 3(a) and 3(b), we compare this theoretical prediction, determined by numerical integration, to our BD simulations, where the effective diffusion coefficient is determined by analyzing the mean-squared displacement of the point particles. In Fig. 3(a), D_{TD}/D is plotted against Pe_u for $\text{Sh} = 0$ and $\text{Pe}_v = \{5, 10, 15, 20\}$; as expected, we observe that $D_{\text{TD}}/D \sim \text{Pe}_u^2$, where the constant of proportionality depends on Pe_v . In Fig. 3(b), D_{TD}/D is now plotted against Pe_v for $\text{Sh} = 0$ and $\text{Pe}_u = 10$, highlighting the complex nonmonotonic dependence of D_{TD}/D on Pe_v . We note that as Pe_v becomes large, the time step dt used in our BD simulation must become smaller and smaller to accurately sample the region near the wall; hence, we do not show simulation results beyond $\text{Pe}_v = 20$.

C. The effective velocity

We may now examine how the $\partial \langle uC \rangle / \partial \bar{x}$ term in Eq. (11) affects the effective advective velocity. In particular, by substituting the portion of the concentration in Eq. (18) that depends on $\langle C \rangle$ into this term, we arrive at an advection term $\langle u \rangle_{\text{eff}} \partial \langle C \rangle / \partial x$, where the effective velocity is

$$\langle u \rangle_{\text{eff}} = \int_0^1 u(y) \mathcal{P}(y) dy + \text{Sh} \int_0^1 u(y) \mathcal{P}(y) \mathcal{Q}(y) dy. \quad (21)$$

By integrating, we have

$$\langle u \rangle_{\text{eff}} = 6 \frac{\text{coth}(\text{Pe}_v/2) + \text{coth}(\text{Re}_v/2)}{\text{Pe}_v + \text{Re}_v} - \frac{12}{\text{Pe}_v \text{Re}_v}, \quad \text{Sh} = 0, \quad (22)$$

when $\text{Sh} = 0$. The $O(\text{Sh})$ correction can also be similarly integrated, but we omit the final expression here due to its length. In Fig. 4(a) we compare this theoretical prediction to our BD simulations; $\langle u \rangle_{\text{eff}}$ is plotted against Pe_v for $\text{Pe}_u = 10$. $\langle u \rangle_{\text{eff}}$ is measured in BD simulation by determining the average velocity of the mean x coordinate of all particles. We only show results for $\text{Sh} = 0$, since we find that the $O(\text{Sh})$ correction is small. For example, when $\text{Re}_v = 1$, we find that the ratio of the second integral to the first integral in Eq. (21) is $O(10^{-2})$; since the result is also only formally valid

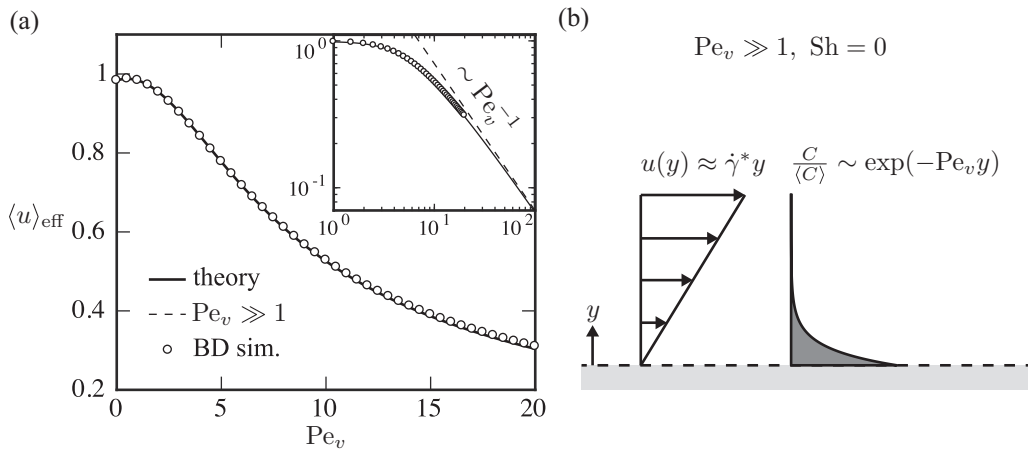


FIG. 4. (a) The effective advective velocity $\langle u \rangle_{\text{eff}}$ when $Re_v = 1$ is shown as function of Pe_v . The inset shows the asymptotic behavior of the velocity when $Pe_v \gg 1$. (b) Schematic describing the asymptotic analysis performed when $Pe_v \gg 1$. The velocity profile is approximated as a simple shear flow.

when $Sh \ll 1$, this small quantity is difficult to extract from simulation. As observed in Fig. 2(a), the concentration profile is pushed closer to the bottom wall as the strength of the cross flow Pe_v increases. As a result, the effective velocity $\langle u \rangle_{\text{eff}}$ decreases as slow velocities near the wall are sampled by the concentration profile.

D. Asymptotic analysis for strong cross flow

The zeroth-order concentration profile is simply $C_0 \sim \langle C \rangle \exp(-Pe_v y)$, and as a result, when $Pe_v \gg 1$, a concentration boundary layer of thickness Pe_v^{-1} forms at the bottom wall. Here we provide an asymptotic analysis of the effective diffusion coefficient and effective velocity in the presence of strong cross flow. When $Pe_v \gg 1$, the majority of the scalar is within a layer of thickness Pe_v^{-1} . As illustrated in Fig. 4(b), within this layer, we can approximate the full velocity profile given in Eq. (5) as a simple shear flow,

$$u(y) \approx \dot{\gamma}^* y, \quad Pe_v \gg 1, \quad (23)$$

where $\dot{\gamma}^* = -12/Re_v + 12/[1 - \exp(-Re_v)]$ is the dimensionless shear rate at the wall. By repeating the preceding analysis with this shear flow and allowing integrals in y to extend to ∞ where there is essentially no scalar, we find that when $Sh = 0$,

$$\frac{D_{\text{TD}}}{D} \approx 2\dot{\gamma}^{*2} Pe_u^2 Pe_v^{-4}, \quad Pe_v \gg 1, \quad Sh = 0, \quad (24)$$

$$\langle u \rangle_{\text{eff}} \approx \dot{\gamma}^* Pe_v^{-1}, \quad Pe_v \gg 1, \quad Sh = 0. \quad (25)$$

In the insets of Figs. 3(b) and 4(a), we show our results for D_{TD}/D and $\langle u \rangle_{\text{eff}}$ on a log scale, and the asymptotic results shown in Eqs. (24) and (25) are shown as dashed lines. Indeed, when $Pe_v \gg 1$, these results are accurate approximations of the full theory, where BD simulations are difficult to

conduct due to the prohibitively small time steps needed. Dimensionally, Eqs. (24) and (25) are

$$D_{\text{TD}} \approx 2\dot{\gamma}^2 D^3 V^{-4}, \quad \text{Pe}_v \gg 1, \quad \text{Sh} = 0, \quad (26)$$

$$\langle u \rangle_{\text{eff}} \approx \dot{\gamma} D V^{-1}, \quad \text{Pe}_v \gg 1, \quad \text{Sh} = 0. \quad (27)$$

Interestingly, our results indicate that in this regime of strong cross flow, the Taylor dispersion coefficient scales dimensionally with the Brownian diffusivity as $D_{\text{TD}} \sim D^3$. This is in contrast to the classical case with no cross flow, where $D_{\text{TD}} \sim D^{-1}$.

While we have been able to determine the asymptotic Taylor dispersion coefficient by direct calculation, we now describe how the scaling in Pe_v can also be revealed by a simple heuristic argument. As noted previously, in the absence of cross flow, the dispersion coefficient in plane Poiseuille flow simply scales with the square of the Péclet number, where velocity and length scales are U and H , respectively. In the presence of strong cross flow, the dispersion coefficient indeed still scales with the square of the Péclet number, but with different velocity and length scales; U and H are no longer the correct scales. In particular,

$$\frac{D_{\text{TD}}}{D} \sim \left(\frac{\Delta U}{U} \frac{\Delta y}{H} \right)^2, \quad \text{Pe}_v \gg 1, \quad \text{Sh} = 0, \quad (28)$$

where Δy is the thickness of the thin concentration layer and ΔU is the velocity difference across the concentration layer. We can approximate this velocity difference as $\Delta U \approx B(\Delta y)^n$, i.e., the first term in the Taylor series for the velocity difference, with n depending on the location of the thin layer. In the problem considered here, the dimensional thickness of the concentration layer is $\Delta y = D/V$ and the local flow is a shear flow with $n = 1$ and $B = \dot{\gamma}$. Substitution into Eq. (28) immediately yields $D_{\text{TD}}/D \sim \dot{\gamma}^2 \text{Pe}_v^2 \text{Pe}_v^{-4}$, which is the result obtained in Eq. (24). This procedure reveals the scalings, but the coefficient, “2,” can only be determined by the full analysis above. For more complex scenarios, such as the case where the cross-flow velocity is spatially nonuniform, this type of argument is valuable since it quickly uncovers the scaling in Pe_v for $\text{Pe}_v \gg 1$. In Sec. III G, we will use this argument again in a slightly more complicated situation.

E. The effective Sherwood number

By evaluating the concentration field given in Eq. (18) at the wall, $y = 0$, we determine the effective Sherwood number Sh_{eff} to be

$$\text{Sh}_{\text{eff}} = \text{Sh}\mathcal{P}(0) + \text{Sh}^2\mathcal{P}(0)\mathcal{Q}(0) \quad (29a)$$

$$= \text{Sh} \left[\frac{\text{Pe}_v}{1 - \exp(-\text{Pe}_v)} \right] - \text{Sh}^2 \left[\frac{\text{Pe}_v}{1 - \exp(-\text{Pe}_v)} \right] \left\{ \frac{\text{Pe}_v - \sinh(\text{Pe}_v)}{[1 - \cosh(\text{Pe}_v)]\text{Pe}_v} \right\}, \quad (29b)$$

which has the limiting behavior

$$\text{Sh}_{\text{eff}} \approx \left(1 + \frac{\text{Pe}_v}{2} \right) \left(\text{Sh} - \frac{1}{3}\text{Sh}^2 \right), \quad \text{Pe}_v \ll 1, \quad \text{Sh} \ll 1, \quad (30a)$$

$$\text{Sh}_{\text{eff}} \approx \text{Pe}_v \text{Sh} - \text{Sh}^2, \quad \text{Pe}_v \gg 1, \quad \text{Sh} \ll 1. \quad (30b)$$

In Figs. 5(a) and 5(b), Sh_{eff} as shown in Eq. (29b) is plotted against Sh for $\text{Pe}_v = \{0, 1, 2\}$ and against Pe_v for $\text{Sh} = \{0.2, 0.4, 0.6, 0.8, 1.0\}$, respectively. Sh_{eff} is measured in BD simulations by fitting an exponential to the number of particles that have not yet transferred.

As the strength of the cross flow Pe_v increases, we observe that Sh_{eff} increases, due to the fact that the scalar is pushed closer to the lower wall. In Fig. 5(a), we show our results both with and without the $O(\text{Sh}^2)$ correction. At zeroth order, the effective Sherwood number is simply $\text{Sh}\mathcal{P}(0)$. However, as scalar is transferred out of the channel, the next order correction leads to a decrease in

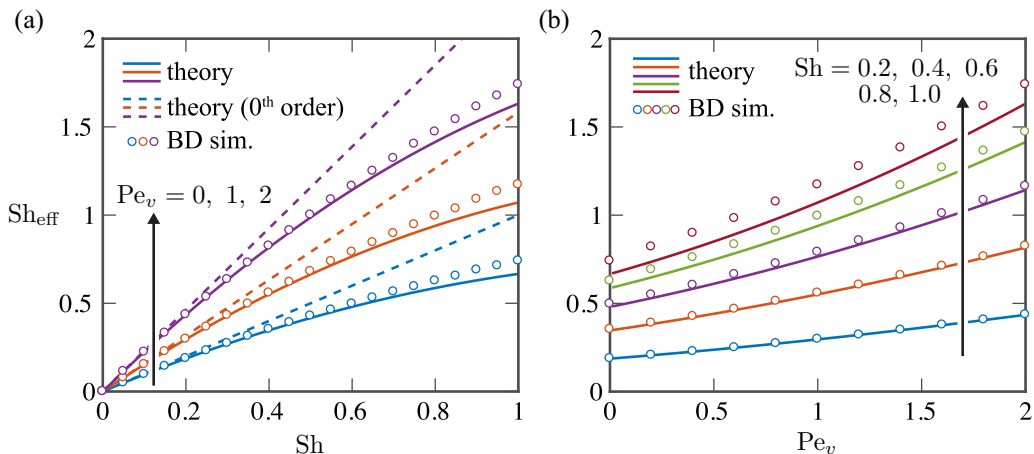


FIG. 5. Effective Sherwood numbers Sh_{eff} when $Pe_u = 10$ and $Re_v = 1$ are shown as functions of (a) Sh , for $Pe_v = \{0, 1, 2\}$, and (b) Pe_v , for $Sh = \{0.2, 0.4, 0.6, 0.8, 1.0\}$.

Sh_{eff} ; this is consistent with the concentration profiles shown in Fig. 2(b), where an increase in Sh leads to a depletion of scalar near the wall. Even though our perturbation theory is only formally valid at $Sh \ll 1$, we observe reasonable agreement with our BD simulations up to $Sh = 1$. We note that in order to study the case where $Sh \gg 1$, which we do not consider in this work, it would be important to consider a higher order perturbation in δ to capture details at short time. With very strong mass transfer, the solute would be removed from the fluid before the long-time Taylor limit is reached.

F. The effect of the Schmidt number

So far, we have studied the effect of varying Pe_v while holding $Re_v = 1$ constant. In doing so, we have implicitly varied the Schmidt number, since $Pe_v = Re_v Sc$, and changes in Pe_v have not affected the axial velocity profile $u(y)$. We now discuss the effect of explicitly varying Sc . At a constant Sc , an increase in the cross-flow strength Pe_v now increases Re_v accordingly, pushing the maximum of $u(y)$ closer to the bottom wall into the concentration boundary layer.

In Fig. 6(a), D_{TD}/D is again plotted against Pe_v when $Pe_u = 10$, but now holding the Schmidt number constant at $Sc = \{0.1, 0.3, 1, 3, 10, 30, 100\}$. At a fixed Sc , we define the maximum dispersion coefficient measured by numerical integration of Eq. (20) as D_{TD}^*/D and the Pe_v corresponding to this maximum as Pe_v^* . In Figs. 6(b) and 6(c), D_{TD}^*/D and Pe_v^* are plotted against Sc , again when $Pe_u = 10$. We observe three different regimes of behavior: (1) At large values of Sc ($Sc \gtrsim 10$), we observe that D_{TD}/D first increases with Pe_v , then decreases. Re_v remains small even as Pe_v increases, causing the velocity field to closely resemble Poiseuille flow with the maximum of $u(y)$ close to the center of the channel. As Pe_v increases slightly, the solute is pushed closer to the bottom wall, causing larger velocity gradients to be sampled, leading to an increase in D_{TD}/D . Eventually, as Pe_v continues to increase, much of the solute is now confined to a thin layer near $y = 0$ where the velocity gradient is the highest, however, D_{TD}/D decreases since the differences in velocities being sampled is small. (2) At moderate values of Sc ($Sc \approx 1$), we observe that D_{TD}/D monotonically decreases with Pe_v , and D_{TD}/D is maximized when $Pe_v = 0$. At these values of Sc , Re_v increases modestly with increasing Pe_v , causing the maximum of $u(y)$ to be appreciably pushed towards $y = 0$. Now, as Pe_v increases, the solute is again pushed closer to the bottom wall, but the region of the velocity field where the gradients are small, i.e., close to where $\partial u/\partial y = 0$, is sampled significantly, leading to this decrease in D_{TD}/D . (3) At small values of Sc ($Sc \lesssim 0.1$), interestingly, we observe that D_{TD}/D yet again increases as Pe_v increases slightly,

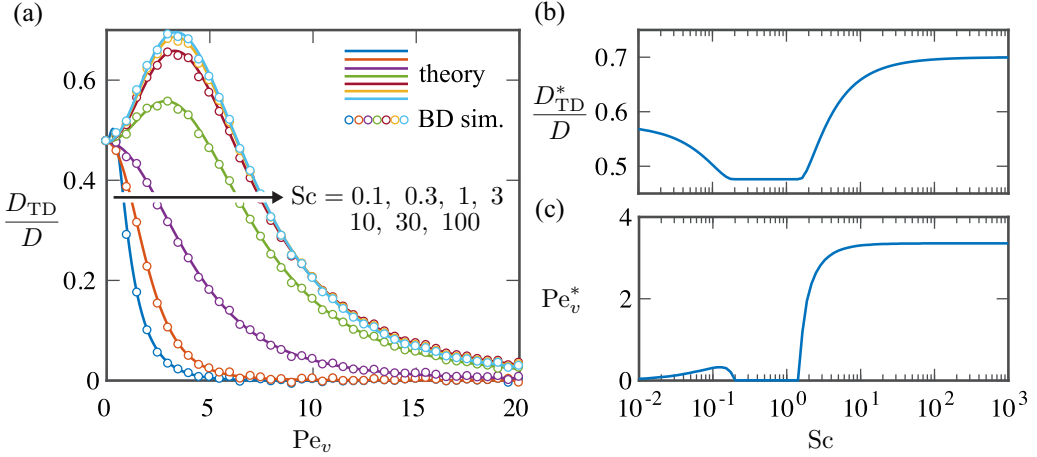


FIG. 6. (a) Taylor dispersion coefficients D_{TD}/D in the absence of mass transfer, $Sh = 0$, are shown as functions of Pe_v , for $Pe_u = 10$ and $Sc = \{0.1, 0.3, 1, 3, 10, 30, 100\}$. (b) The maximum $D_{TD}/D = D_{TD}^*/D$ and (c) corresponding $Pe_v = Pe_v^*$ are plotted as a function of Sc .

and then subsequently decreases. As Sc decreases further, we find that this critical Pe_v becomes very small; we attribute this nonmonotonic behavior to the complex interactions between the thin velocity boundary layer immersed within the concentration boundary layer. It is worth noting that in real systems, however, these small values of Sc are difficult to obtain.

In the limit that $Sc = \infty$, we must have $Re_v = 0$ for any Pe_v , and the velocity field is simple Poiseuille flow. In this limit, we see that the dispersion coefficient approaches $D_{TD}^*/D \approx 0.7$, corresponding to $Pe_v^* \approx 3.4$, a nearly 50% increase from the dispersivity measured when $Pe_v = 0$. This limit of infinite Schmidt number corresponds to the example of sedimenting Brownian particles considered by Shapiro and Brenner [15], where the driving force for transverse motion does not affect the axial velocity profile of the solvent. In that work, they report an increase in D_{TD}/D with increasing Pe_v (i.e., increasing gravity), up to $Pe_v = 2$, but they do not discuss the subsequent decrease in D_{TD}/D at larger Pe_v . Clearly, for most values of Pe_v and Sc the dispersion coefficient D_{TD}/D decreases from its small Pe_v value. In general, this limit of infinite Sc represents an applied external field that drives transverse motion, and these results may be useful in understanding, for instance, how an applied magnetic field affects the axial dispersion of magnetic nanoparticles in a blood vessel network.

The asymptotic relations given in Eqs. (24) and (25) still hold here at large fixed Sc , when the concentration boundary layer is very thin compared to the momentum boundary layer. However, the scalings in Pe_v are not as simple: at a fixed Sc , the wall shear rate $\dot{\gamma}^*$ is now a function of Pe_v . By expanding the wall shear rate around $Pe_v^{-1} = 0$ at a fixed Sc , we have

$$\dot{\gamma}^* = 12 - 12 Sc Pe_v^{-1} + O(Pe_v^{-2}), \quad Pe_v \gg 1. \quad (31)$$

At a small fixed Sc , we expect our asymptotic analysis to break down however. The velocity field given in Eq. (5) is maximized at y^* , which is $1/2$ when $Pe_v = 0$ and goes to 0 as $Pe_v \rightarrow \infty$. At small values of Sc , y^* can be even smaller than Pe_v^{-1} ; in other words, the momentum boundary layer can be even thinner than the concentration boundary layer. Certainly, the approximation that the velocity field is a simple shear flow is no longer valid here, and as we have seen in Fig. 6, nontrivial behavior occurs when the momentum boundary layer is much thinner than the concentration boundary layer. Notably, this nontrivial dependence on the Schmidt number is the result of having a velocity profile $u(y)$ that has a shear rate that varies in y ; in the case of a simple shear flow across the entire width of the channel, there would be no boundary layer in momentum.

G. Spatially nonuniform transverse velocity and diffusivity

We have thus far focused on the dispersion of particles in the presence of a spatially uniform cross flow. In using this simple cross flow, we have elucidated how transverse motion affects Taylor dispersion. Of course, most transverse flows are not spatially uniform, and in fact, in many applications the particle velocity \mathbf{u}_p will not necessarily be equal to the fluid velocity \mathbf{u} . We have introduced the subscript “p” (particle) to highlight this distinction. Note that while the velocity field of an incompressible fluid must be divergence-free, the same is not required of the particle velocity, since particles can accumulate. Similarly, the diffusion coefficient D , which so far has been considered to be a constant, could also vary spatially and thus capture more general diffusive effects [26,27]. In this section, we show how our analysis changes when the transverse particle velocity is $v_p = v_p(y)$ and the diffusivity is $D_p = D_p(y)$. We describe various applications where this situation arises, and we focus on the illustrative phenomenon of the lateral migration of particles in a viscoelastic flow.

We repeat the Taylor dispersion analysis with $v_p = v_p(y)$ and $D_p = D_p(y)$ when $Sh = 0$. Again, the velocity $v_p(y)$ and diffusivity $D_p(y)$ are nondimensionalized with characteristic scales V and D , so that the Péclet number is $Pe_v = VH/D$. At $O(1)$, we still have the concentration field $C_0 = (C)\mathcal{P}(y)$, except instead of Eq. (15), the weighting function is

$$\mathcal{P}(y) = \frac{\exp\left[Pe_v \int_0^y \frac{v_p(\eta)}{D_p(\eta)} d\eta\right]}{\int_0^1 \exp\left[Pe_v \int_0^y \frac{v_p(\eta)}{D_p(\eta)} d\eta\right] dy}. \quad (32)$$

Moreover, instead of Eq. (20), the Taylor dispersion coefficient is

$$\begin{aligned} \frac{D_{TD}}{D} &= -Pe_u^2 \int_0^1 \tilde{u}_p(y) \exp\left[Pe_v \int_0^y \frac{v_p(\eta)}{D_p(\eta)} d\eta\right] \\ &\quad \times \left\{ \int_0^y \exp\left[-Pe_v \int_0^\sigma \frac{v_p(\eta)}{D_p(\eta)} d\eta\right] \left[\int_0^\sigma \mathcal{P}(\xi) \tilde{u}_p(\xi) d\xi \right] d\sigma \right\} dy. \end{aligned} \quad (33)$$

Spatially nonuniform transverse velocities and diffusivities arise in a number of applications. In the channel flow of blood—a multicomponent suspension mainly comprising deformable red blood cells and more rigid platelets and white blood cells—it is well known that red blood cells experience a migration velocity away from the walls due to their deformability. Additionally, hydrodynamic collisions between the components cause a spatially nonuniform shear-induced diffusivity and transverse drift velocity [18,28]. A shear-induced diffusivity also arises in a sheared concentrated hard sphere suspension [29], although with hard spheres, multibody interactions drive this effect, whereas only pairwise interactions are required for deformable particles. In the pressure-driven flow through a channel where fluid weakly leaks out of both walls at a specified velocity, a Berman flow [30], the transverse fluid velocity is expressed as a perturbation series in the leakage Reynolds number.

We now describe an analytically tractable application that highlights how having $v_p = v_p(y)$ can affect Taylor dispersion. In the channel flow of a particle-laden viscoelastic fluid, Li and Xuan [31] experimentally showed that an external force applied to the particles in the direction of flow causes particles to drift toward the channel center, while a force opposing the direction of flow causes particles to drift toward the channel walls. Einarsson and Mehlig [32] investigated this effect theoretically, and showed that to first order in the Weissenberg number (the product of the polymer relaxation time and the characteristic shear rate), this drift velocity is proportional to the local shear rate of the flow. For an Oldroyd-B fluid, the axial velocity profile is the same as the Newtonian solution $u = 6y(1 - y)$, so that the shear rate is $\partial u/\partial y \sim 1 - 2y$. Thus, we investigate the Taylor dispersion of particles in a pressure-driven flow with a transverse velocity given by

$$v_p(y) = \pm(1 - 2y), \quad (34)$$

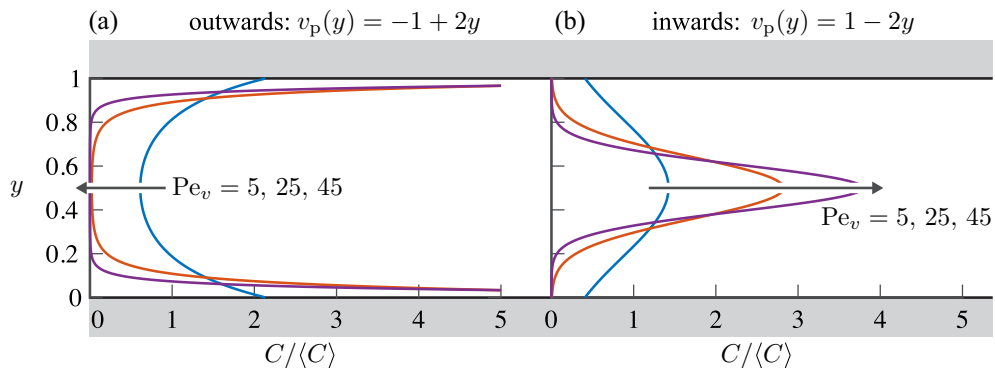


FIG. 7. Concentration profiles $C/\langle C \rangle$ are shown for $Pe_v = \{5, 25, 45\}$ when the transverse particle velocity is (a) outwards, $v_p(y) = -1 + 2y$, and (b) inwards, $v_p(y) = 1 - 2y$.

where the “+” corresponds to a force causing the particles to drift inwards toward the channel center, and the “−” corresponds to a force causing the particles to drift outwards toward the channel walls. Here, while the transverse fluid velocity is $v = 0$, the transverse particle velocity v_p is given by Eq. (34). Note that a drift dependent on the shear rate occurs in other contexts as well, such as the deformation-induced wall drift experienced by capsules [33], vesicles [34], and polymers [35]. In Figs. 7(a) and 7(b), we show concentration profiles induced by the drift velocity in Eq. (34) as a function of y at the center of the Gaussian by evaluating the weighting function $\mathcal{P}(y)$ given in Eq. (32); this shows that $C_0 \sim \langle C \rangle \exp[\pm Pe_v(y - y^2)]$. Figures 7(a) and 7(b) show $C/\langle C \rangle$ when the transverse particle velocity is outward and inward, and as expected, as Pe_v increases, the concentration either gets pushed closer to the channel walls or to the channel center, respectively.

Based on this solution for the concentration field, we may now examine the Taylor dispersion coefficient and effective streamwise velocity with these transverse particle velocities. In Fig. 8(a), we show the Taylor dispersion coefficient D_{TD}/D for $Pe_u = 10$ as a function of Pe_v for both the outward and inward transverse particle velocities, determined by numerical integration of Eq. (33). Interestingly, while the outward particle velocity leads to a nonmonotonic dependence of D_{TD}/D

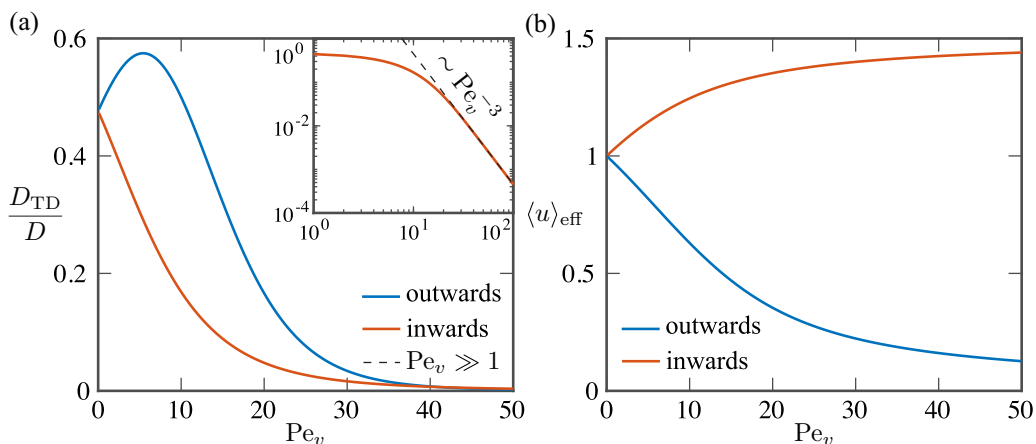


FIG. 8. (a) Taylor dispersion coefficients D_{TD}/D as a function of Pe_v for $Pe_u = 10$ for both the outward and inward particle velocities. The inset shows the asymptotic behavior of the dispersion coefficient when $Pe_v \gg 1$ for the inward particle velocity. (b) Effective velocity $\langle u \rangle_{\text{eff}}$ as a function of Pe_v for both the outward and inward particle velocities.

on Pe_v , the Taylor dispersion coefficient in the presence of inward particle velocity decreases monotonically. In Fig. 8(b), the effective velocity $\langle u \rangle_{\text{eff}}$ is plotted against Pe_v . As Pe_v increases, the outward particle velocity pushes the concentration profile closer to the walls where the velocity is slow, leading to a reduction in $\langle u \rangle_{\text{eff}}$. In contrast, an inward transverse particle velocity pushes the concentration profile toward the channel center, where the velocity is maximum, causing $\langle u \rangle_{\text{eff}}$ to approach the maximum velocity of $3/2$.

In the limit of strong outward transverse particle velocity, we expect the previous asymptotic analysis [Eqs. (24)–(27)] to hold. As before, we have a concentration boundary layer of thickness Pe_v^{-1} immersed in a wall shear flow, since the outward velocity is a constant near the wall. However, the asymptotic analysis for strong inward transverse particle velocity predicts scalings which are qualitatively different. By switching to a wall-normal coordinate centered in the middle of the channel, $y' = y - 1/2$, we see that the inward velocity field is $v_p(y') = -2y'$, and thus, the concentration field is given by $C_0 \sim \langle C \rangle \exp(-Pe_v y'^2)$. This shows that the thickness of the concentration layer is $Pe_v^{-1/2}$. At the center of the channel, where the majority of the particles are concentrated, the velocity profile is the quadratic profile $u = -6y'^2 + 3/2$, and this must be considered in the asymptotic analysis. By repeating the Taylor dispersion analysis in the thin center layer and allowing integrals in y' to extend to plus and minus infinity, we find that

$$\frac{D_{\text{TD}}}{D} \approx \frac{9}{2} Pe_u^2 Pe_v^{-3}, \quad Pe_v \gg 1, \quad Sh = 0, \quad (35)$$

$$\langle u \rangle_{\text{eff}} \approx \frac{3}{2} - 3Pe_v^{-1}, \quad Pe_v \gg 1, \quad Sh = 0. \quad (36)$$

Notably, the dispersion coefficient now decays as Pe_v^{-3} instead of Pe_v^{-4} as before. In the inset of Fig. 8(a), the results for dispersion in the presence of inward particle velocity are plotted on a log scale, and the asymptotic result shown in Eq. (35) is presented as a dashed line. Importantly, this scaling could have also been revealed using the previous heuristic argument. The dimensional thickness of the concentration layer is $\Delta y = \sqrt{DH/V}$, and since the flow is quadratic at the center, $n = 2$. Substitution into Eq. (28) yields $D_{\text{TD}}/D \sim Pe_u^2 Pe_v^{-3}$, which aside from the $9/2$ coefficient, is the result in Eq. (35). By applying our results to the lateral migration of particles in a viscoelastic flow, we have thus underscored the mechanism by which different transverse velocities can affect dispersion behavior.

IV. CONCLUDING REMARKS

In this work, we have used both perturbation theory and Brownian dynamics simulations to study the effect of cross flow and wall mass transfer on Taylor dispersion. By perturbing the concentration field to $O(\delta)$, we have provided a useful formula for the Taylor dispersion coefficient as a function of Pe_v . By perturbing the concentration field to $O(Sh)$, where the dispersion coefficient is not affected, we have provided useful formulas for the effective velocity of $\langle C \rangle$ to $O(Sh)$ and the effective Sherwood number to $O(Sh^2)$. Additionally, we have conducted an asymptotic analysis of the problem in the regime of strong cross flow, or $Pe_v \gg 1$. Furthermore, we have discussed the effect of the Schmidt number on the dispersion coefficient. Finally, we described how our results can be extended to take into account a nonuniform transverse velocity and diffusivity.

In order to illustrate how our results may be used, we conclude with a practical engineering example. In cross-flow filtration of particles or molecules in fluid, the larger particles that do not pass through the filter—the retentate—form a thin cake layer on the membrane surface. The thickness of the cake layer determines the flux of the permeate through the filter, and one may ultimately be interested in how this flux varies along the filter. In order to evaluate the performance of this filtration system, the axial dispersion coefficients of both the smaller permeate and larger retentate as a function of the pressure difference across the filter would be of interest. Typical Schmidt numbers vary widely. For example, in air, gaseous species have $Sc = O(1)$, while solid

particles with radii ranging from 0.001 to 10 μm have $Sc = O(10^1)$ to $O(10^7)$ [36]. In water, where typical solutes encountered in cross-flow filtration systems vary from small molecules, such as salts, to large particles, such as cells, the Brownian diffusion coefficient can vary from $O(10^{-14})$ to $O(10^{-9})$ m^2/s [37], leading to typical Schmidt numbers of $Sc = O(10^3)$ to $O(10^8)$. By tuning the pressure difference across the filter to select a cross-flow Péclet number Pe_v , one could then use the results of Fig. 6 to estimate the appropriate dispersion coefficient.

While our results are directly applicable to mass-transfer problems such as cross-flow filtration, it is interesting to note that our results could also extend to problems involving Taylor dispersion of heat in the presence of cross flow. The equations of mass and heat transfer are equivalent, where the scalar of interest is now temperature, the Brownian diffusivity is replaced with the thermal diffusivity, and mass transfer corresponds to convective heat transfer. The Prandtl number Pr , which replaces the Schmidt number, now represents the relative thicknesses of the momentum and thermal boundary layers. At room temperature, common gases have $Pr = O(1)$ while common liquids such as water and oils have $Pr = O(1)$ to $O(10^3)$. Our results are thus also applicable in problems where the rate that heat is transported axially in a fluid flowing between two porous insulated plates with a supplied cross flow is of interest.

ACKNOWLEDGMENTS

The authors thank Prof. A. Acrivos for providing many useful comments and suggestions on our work, and T.Y.L. thanks Dr. J. Einarsson for many fruitful conversations about Taylor dispersion. Computer simulations were performed on the Stanford University Certainty computer cluster, which is funded by the American Recovery and Reinvestment Act of 2009.

-
- [1] G. I. Taylor, Dispersion of soluble matter in solvent flowing slowly through a tube, *Proc. R. Soc. London A* **219**, 186 (1953).
 - [2] R. Aris, On the dispersion of a solute in a fluid flowing through a tube, *Proc. R. Soc. London A* **235**, 67 (1956).
 - [3] G. I. Taylor, The dispersion of matter in turbulent flow through a pipe, *Proc. R. Soc. London A* **223**, 446 (1954).
 - [4] A. Nadim, R. G. Cox, and H. Brenner, Transport of sedimenting Brownian particles in a rotating Poiseuille flow, *Phys. Fluids* **28**, 3457 (1985).
 - [5] M. E. Erdogan and P. C. Chatwin, The effects of curvature and buoyancy on the laminar dispersion of solute in a horizontal tube, *J. Fluid Mech.* **29**, 465 (1967).
 - [6] S. C. James and C. V. Chrysikopoulos, Effective velocity and effective dispersion coefficient for finite-sized particles flowing in a uniform fracture, *J. Colloid Interf. Sci.* **263**, 288 (2003).
 - [7] C.-O. Ng, Dispersion in steady and oscillatory flows through a tube with reversible and irreversible wall reactions, *Proc. R. Soc. London A* **462**, 481 (2006).
 - [8] R. Sankarasubramanian and W. N. Gill, Unsteady convective diffusion with interphase mass transfer, *Proc. R. Soc. London A* **333**, 115 (1973).
 - [9] P. S. Gupta and A. S. Gupta, Effect of homogeneous and heterogeneous reactions on the dispersion of a solute in the laminar flow between two plates, *Proc. R. Soc. London A* **330**, 59 (1972).
 - [10] B. Berkowitz and J. Zhou, Reactive solute transport in a single fracture, *Water Resour. Res.* **32**, 901 (1996).
 - [11] A. E. De Gance and L. E. Johns, On the dispersion coefficients for Poiseuille flow in a circular cylinder, *Flow Turbul. Combust.* **34**, 227 (1978).
 - [12] A. E. De Gance and L. E. Johns, The theory of dispersion of chemically active solutes in a rectilinear flow field, *Flow Turbul. Combust.* **34**, 189 (1978).

- [13] M. Shapiro and H. Brenner, Taylor dispersion of chemically reactive species: irreversible first-order reactions in bulk and on boundaries, *Chem. Eng. Sci.* **41**, 1417 (1986).
- [14] I. Frankel and H. Brenner, On the foundations of generalized Taylor dispersion theory, *J. Fluid Mech.* **204**, 97 (1989).
- [15] M. Shapiro and H. Brenner, Chemically reactive generalized Taylor dispersion phenomena, *AIChE J.* **33**, 1155 (1987).
- [16] R. H. Davis and J. D. Sherwood, A similarity solution for steady-state crossflow microfiltration, *Chem. Eng. Sci.* **45**, 3203 (1990).
- [17] R. K. Jain and T. Stylianopoulos, Delivering nanomedicine to solid tumors, *Nature Rev. Clin. Oncol.* **7**, 653 (2010).
- [18] Q. M. Qi and E. S. G. Shaqfeh, Theory to predict particle migration and margination in the pressure-driven channel flow of blood, *Phys. Rev. Fluids* **2**, 093102 (2017).
- [19] C.-H. Heldin, K. Rubin, K. Pietras, and A. Östman, High interstitial fluid pressure—An obstacle in cancer therapy, *Nature Rev. Cancer* **4**, 806 (2004).
- [20] A. D. Grief and G. Richardson, Mathematical modelling of magnetically targeted drug delivery, *J. Magn. Mater.* **293**, 455 (2005).
- [21] J. Dobson, Magnetic nanoparticles for drug delivery, *Drug Dev. Res.* **67**, 55 (2006).
- [22] P. N. Shah, T. Y. Lin, I. L. Aanei, S. H. Klass, B. R. Smith, and E. S. G. Shaqfeh, Extravasation of Brownian spheroidal nanoparticles through vascular pores, *Biophys. J.* **115**, 1103 (2018).
- [23] G. K. Batchelor, *An Introduction to Fluid Dynamics* (Cambridge University Press, New York, USA, 2000).
- [24] H. C. Öttinger, *Stochastic Processes in Polymeric Fluids: Tools and Examples for Developing Simulation Algorithms* (Springer Science & Business Media, Berlin, Germany, 2012).
- [25] A. Singer, Z. Schuss, A. Osipov, and D. Holcman, Partially reflected diffusion, *SIAM J. Appl. Math.* **68**, 844 (2008).
- [26] I. C. Christov and H. A. Stone, Shear dispersion in dense granular flows, *Granular Matter* **16**, 509 (2014).
- [27] I. M. Griffiths and H. A. Stone, Axial dispersion via shear-enhanced diffusion in colloidal suspensions, *Europhys. Lett.* **97**, 58005 (2012).
- [28] R. G. Henríquez Rivera, X. Zhang, and M. D. Graham, Mechanistic theory of margination and flow-induced segregation in confined multicomponent suspensions: Simple shear and Poiseuille flows, *Phys. Rev. Fluids* **1**, 060501 (2016).
- [29] D. Leighton and A. Acrivos, The shear-induced migration of particles in concentrated suspensions, *J. Fluid Mech.* **181**, 415 (1987).
- [30] A. S. Berman, Laminar flow in channels with porous walls, *J. Appl. Phys.* **24**, 1232 (1953).
- [31] D. Li and X. Xuan, Electrophoretic slip-tuned particle migration in microchannel viscoelastic fluid flows, *Phys. Rev. Fluids* **3**, 074202 (2018).
- [32] J. Einarsson and B. Mehlig, Spherical particle sedimenting in weakly viscoelastic shear flow, *Phys. Rev. Fluids* **2**, 063301 (2017).
- [33] H. Zhao, E. S. G. Shaqfeh, and V. Narsimhan, Shear-induced particle migration and margination in a cellular suspension, *Phys. Fluids* **24**, 011902 (2012).
- [34] H. Zhao, A. P. Spann, and E. S. G. Shaqfeh, The dynamics of a vesicle in a wall-bound shear flow, *Phys. Fluids* **23**, 121901 (2011).
- [35] D. Saintillan, E. S. G. Shaqfeh, and E. Darve, Effect of flexibility on the shear-induced migration of short-chain polymers in parabolic channel flow, *J. Fluid Mech.* **557**, 297 (2006).
- [36] B. B. Hicks, D. D. Baldocchi, T. P. Meyers, R. P. Hosker, and D. R. Matt, A preliminary multiple resistance routine for deriving dry deposition velocities from measured quantities, *Water Air Soil Poll.* **36**, 311 (1987).
- [37] P. Aimar, M. Meireles, P. Bacchin, and V. Sanchez, Fouling and concentration polarization in ultrafiltration and microfiltration, in *Membrane Processes in Separation and Purification*, edited by J. G. Crespo and K. W. Böddeker (Springer, Dordrecht, 1994), pp. 27–57.